Abstract #947, 224th ECS Meeting, © 2013 The Electrochemical Society

Potential dependence of electrochemical behavior of Porous Electrodes for Li-ion Batteries

Nobuhiro Ogihara, Yuich Itou, Shigehiro Kawauchi, Tetsuro Kobayashi and Yoji Takeuchi

Toyota Central R&D Labs., Inc., Nagakute, Aichi, 480-1192, Japan

Internal resistance at porous electrodes for Li-ion batteries is a key factor for device power capability. It is difficult to improve the power capability without a full understanding of the electrochemical interfacial phenomena in porous electrodes.

Recently, we reported electrochemical analysis of actual porous electrodes for Li-ion batteries by a combination of EIS using symmetric cells (Fig. 1) and theory of transmission line model (TLM) for cylindrical pores [1, 2]. The individual internal resistance components of the actual porous electrode/electrolyte interface could be categorized as following parameters: electrolyte bulk resistance (R_{sol}), ionic resistance in pores (R_{ion}), and charge-transfer resistance (R_{ct}). These internal resistances are obtained by fitting the experimental impedance plots using TLM for both faradaic and non-faradaic processes. The overall impedances of non-faradaic and faradaic processes are expressed as Eq. 1 and 2, respectively [3-5].

$$Z = R_{sol} + \sqrt{\frac{R_{ion}}{L \cdot j\omega C_{dl}}} \coth \sqrt{R_{ion} L j\omega C_{dl}}\, X \qquad (1)$$

$$Z = R_{sol} + \sqrt{\frac{R_{ion} R_{ct}}{L(1 + j\omega R_{ct} C_{dl})}} \coth \sqrt{\frac{R_{ion} L(1 + j\omega R_{ct} C_{dl})}{R_{ct}}}\, X \qquad (2)$$

(L: pore radius, X: pore length, C_{dl}: double layer capacitance)

Figure 2 shows a comparison of the Nyquist plots obtained by experimental and calculation with state of charge (SOC) = 0 and 50%. Theoretical and experimental impedance behavior results agree with each other. These results indicate that the internal resistances are separated well by the proposed approach. [1]

In this study, we investigated the potential dependence of the internal resistances of the porous electrodes for Li-ion batteries by using our proposed analysis. Figure 3 shows the potential dependence of Nyquist plots at 20°C. At all potential conditions, the plots appear as linear behavior with a 45-degree slop and semi-circle behavior in the high (20 Hz ~ 100 kHz) and low (100 mHz ~ 20 Hz) frequency regions, respectively. Only the semi-circle in the low frequency region varies with changes in potentials. This result indicates that only R_{ct} shows the potential dependence without changing R_{ion}.

From the temperature dependence, a kinetics interpretation of potential dependence for faradaic processes of $LiNiO_2$-based porous electrodes will be discussed.

References

1. Ogihara *et al.*, J. Electrochem. Soc., 159, A1034 (2012).
2. Ogihara *et al.*, Abstract of PRiME2012, #723 (2012).
3. R. D. Levie, Electrochim. Acta, 8, 751 (1963).
4. R. D. Levie, Electrochim. Acta, 9, 1231 (1964).
5. Itagaki *et al.*, *Electrochemistry*, **75**, 649 (2007).

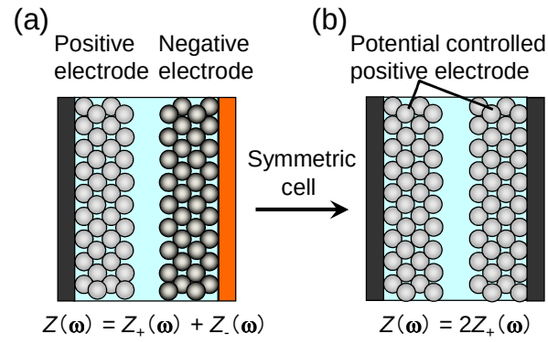

Fig. 1 Schematic cell configurations: (a) asymmetric cell for conventional and classical impedance measurements and (b) symmetric cell with separator including electrolyte for R_{ion} and R_{ct} measurements.

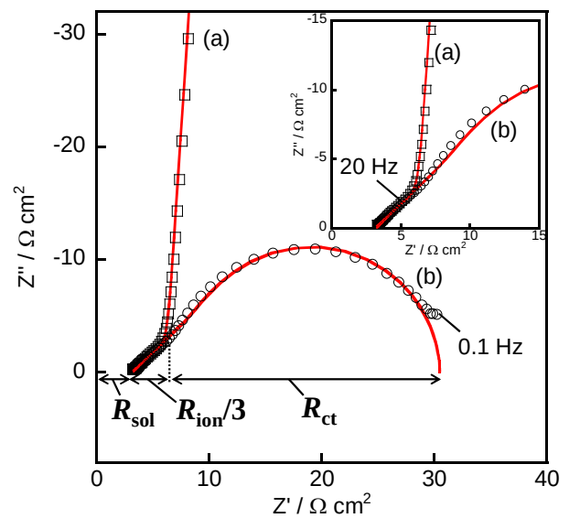

Fig. 2 Nyquist plots for symmetric cells using two $LiNiO_2$-based electrodes in 1.0 M $LiPF_6$ in EC/DMC/EMC (30/40/30) at 20 ˚C. Electrodes prepared at: (a) SOC = 0% (squares) and (b) SOC = 50% (circles). The solid lines are the best-fitted results with the equivalent circuits using Eq. 1 and 2, for (a) and (b), respectively.

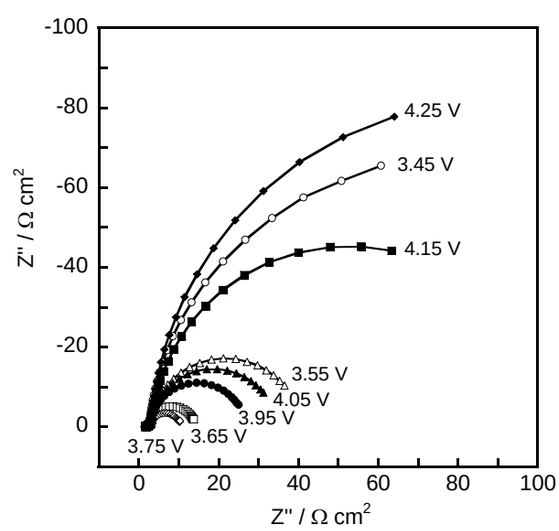

Fig. 3 Nyquist plots for symmetric cells using $LiNiO_2$-based electrodes prepared at different potentials.